How to cite: *Angew. Chem. Int. Ed.* **2024**, *63*, e202314528
doi.org/10.1002/anie.202314528

Analytical Chemistry

Fluorescent-Probe Characterization for Pore-Space Mapping with Single-Particle Tracking

Rafael Mayorga González[+], *J. J. Erik Maris*[+], *Marita Wagner, Yadolah Ganjkhanlou, Johan G. Bomer, Maximilian J. Werny, Freddy T. Rabouw, Bert M. Weckhuysen, Mathieu Odijk, and Florian Meirer**

Abstract: Porous solids often contain complex pore networks with pores of various sizes. Tracking individual fluorescent probes as they diffuse through porous materials can be used to characterize pore networks at tens of nanometers resolution. However, understanding the motion behavior of fluorescent probes in confinement is crucial to reliably derive pore network properties. Here, we introduce well-defined lithography-made model pores developed to study probe behavior in confinement. We investigated the influence of probe-host interactions on diffusion and trapping of confined single-emitter quantum-dot probes. Using the pH-responsiveness of the probes, we were able to largely suppress trapping at the pore walls. This enabled us to define experimental conditions for mapping of the accessible pore space of a one-dimensional pore array as well as a real-life polymerization-catalyst-support particle.

Efficient molecular transport through functional porous solids improves their performance in applications, such as adsorption processes and heterogeneous catalysis.[1] Therefore, pore accessibility and interconnectivity are highly important performance indicators. The pore structure of solid catalysts is often a complex network of macro-, meso-, and micropores with a heterogeneous composition.[2–5] The transition to a more rational pore-space design approach holds great promise for the improvement of catalysts. High-resolution characterization of the pore volume is needed to investigate the relation between synthesis parameters and resulting pore networks. However, this requires complex and expensive analytical techniques such as electron tomography or synchrotron-radiation-based X-ray microscopy.[1,6–10]

A promising approach is to use fluorescent probes. Imaging the uptake of fluorescent probes using confocal laser scanning microscopy has proven effective to reconstruct the probe accessibility in catalysts.[4] However, the resolution of this method (≈250 nm), is limited by the diffraction of light.[11] To overcome this, single-molecule (particle) localization microscopy (SMLM) and single particle tracking (SPT) are promising techniques.[12–18] Fluorescent probes are tracked with a resolution on the order of 10 nm as they diffuse through the pore network, and their trajectories contain information about pore-accessibility and interconnectivity.[15,16] Furthermore, pore size and surface properties might be derived from the duration of trapping events and probe diffusivity, but this has not yet been experimentally demonstrated.[19–21]

To use this approach, one needs to understand the relationship between probe trajectories and the local pore environment. This is non-trivial because single-probe motion in porous materials is heterogeneous and characterized by temporary immobilization ("trapping").[17,22,23] The origin of this heterogeneity is hard to pinpoint because of a catalyst material's complexity. Therefore, a thorough characterization of the probe's motion behavior in well-defined pore structures is essential for proper interpretation of SMLM experiments in complex materials.

Here, we introduce well-defined lithography-made model pores with known geometry and composition to address the challenges outlined above.[24] We first study motion behavior of quantum dots (QDs) using SPT in a two-dimensional (2D) pore, i.e., with confinement in only one direction. The used nanoparticles are promising probes due to their bright fluorescence and small diameter (ca. 15 nm). We investigate the influence of probe-host interactions on diffusion and trapping of single QDs. Based on this characterization, we define a set of experimental conditions that allow the (partial) mapping of two pore systems with increasing levels of complexity: a lithography-made one-

[*] R. M. González,[+] Dr. J. J. E. Maris,[+] M. Wagner, Dr. Y. Ganjkhanlou, Dr. M. J. Werny, Dr. F. T. Rabouw, Prof. B. M. Weckhuysen, Dr. F. Meirer
Inorganic Chemistry and Catalysis, Debye Institute for Nanomaterials Science and Institute for Sustainable and Circular Chemistry, Utrecht University
Universiteitsweg 99, 3584 CG Utrecht (The Netherlands)
E-mail: F.Meirer@uu.nl

Dr. J. G. Bomer, Prof. M. Odijk
BIOS Lab on a Chip Group, MESA+ Institute for Nanotechnology, University of Twente
7522 ME Enschede (The Netherlands)

[+] These authors contributed equally to this work.

dimensional (1D) pore (confinement in two directions) and an industrial olefin polymerization-catalyst-support particle.

The model pore system is a nanofluidic device constructed via microlithography and wet etching from Borofloat glass wafers (Figure 1a). The 2D model pores are slit-shaped patches (depth: 50 nm) imposing confinement only in depth while allowing free diffusion in the plane perpendicular to it. In these two dimensions, we tracked motion of the fluorescent probes while keeping the whole slit within the focal depth of 800 nm (Supporting Information S1).

We tracked polyethylene glycol (PEG)-coated QDs (Figure 1b) suspended in a water/glycerol mixture inside the 2D pore (Figure 1c). The tracks were long compared to previous studies[17] and trajectories displayed permanent, transient, or no trapping (Figure 1d); this behavior was found to be pH dependent. Both probe-wall adsorption and a dramatically increased hydrodynamic drag near the pore wall can cause trapping.[25,26] However, these effects cannot be discriminated with our experiment.

To assess the trapping behavior in confinement, solutions with different pH were loaded in the 2D model pore. Two timeframes were investigated: short trapping events with durations of 5–100 frames (35 ms/frame) and long trapping events lasting more than 100 up to thousands of frames. We identified long trapping events via a 2D histogram of the localization coordinates, which displays the spatial distribution of all localizations during a movie of 4000 frames (Figure 2a,b, Supporting Information S3). Bins with significantly more counts than their direct neighbors indicate trapped particles. The 2D-histogram revealed several long trapping events at 7.5 mM NaOH concentration, while only one was observed at 20 mM NaOH. Unexpectedly, the long-lasting trapping events resulted in artefacts in the trajectory generation process because trajectories belonging to moving particles were often wrongly linked to trapped ones. We therefore removed trajectories close to these locations (Supporting Information S2). This filtering leads to undesired "blind-spots" in the mapped pore space (Figure S6), suggesting that non-trapping probes are preferred to fully map pore spaces.

Next, we analyzed short trapping events within trajectories (Supporting Information S4).[24,27–29] This difference can be explained by increased electrostatic repulsion between QDs and a silica pore wall at increasing pH (Supporting Information S5). This repulsion prevents the QD from getting close enough to the silica where probe-wall attraction and/or hydrodynamic drag dominate. To cross-check

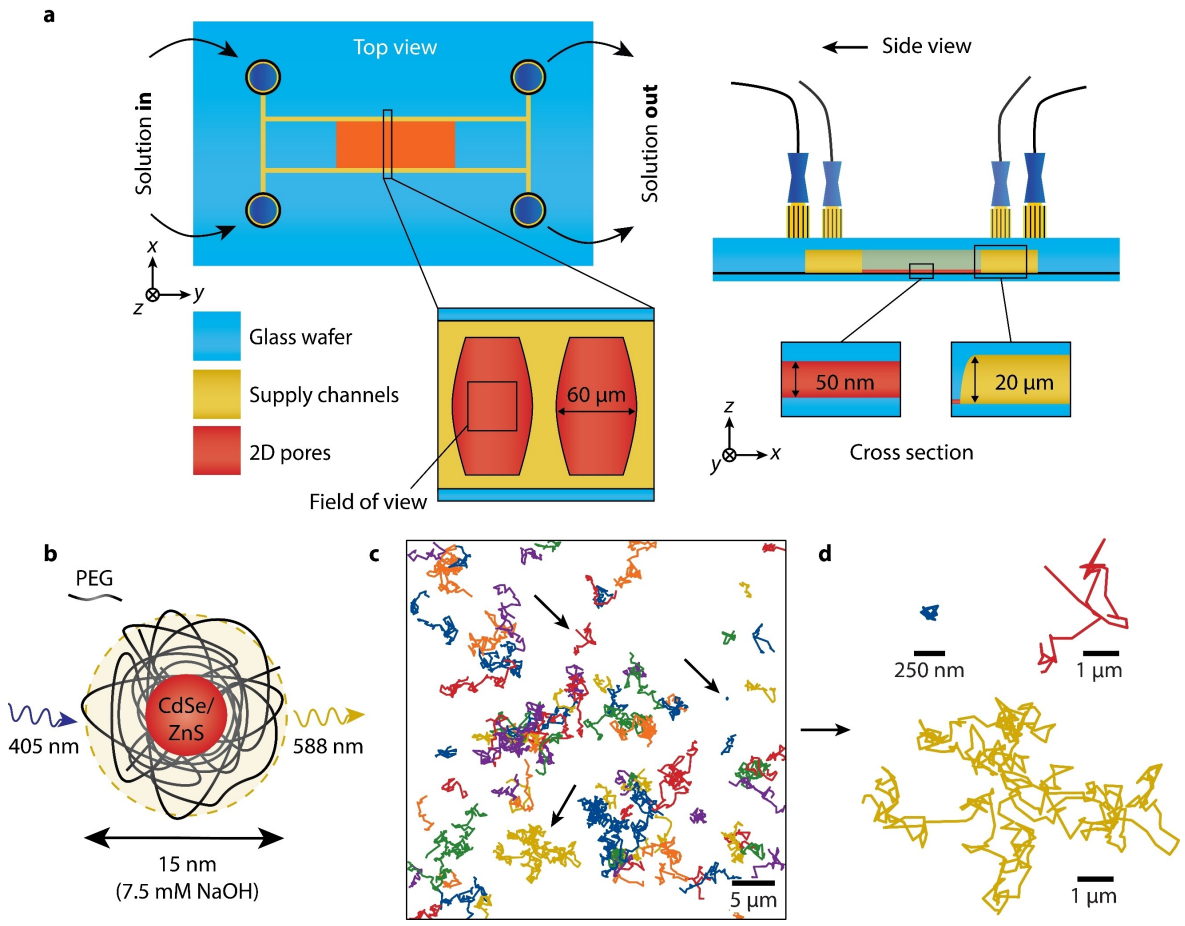

Figure 1. a) Schematic representation of the nanofluidic device. b) PEG-coated CdSe/ZnS QDs. c) Selection of observed trajectories within the field of view. d) Three enlarged trajectories, marked by arrows in (c).

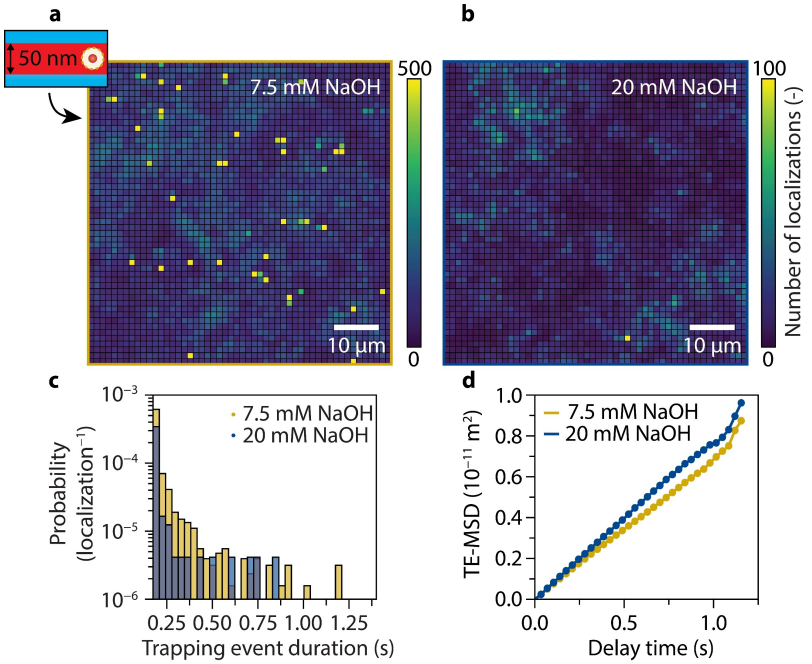

Figure 2. a,b) 2D histogram of the single-particle coordinates in the 2D pore during 4000 frames in (a) 7.5 mM and (b) 20 mM NaOH; bin-size: 0.87×0.87 µm^2. The color coding gives the localizations per 4000 frames. The 7.5 mM NaOH sample had an additional 2.5 mM NaCl to keep the Debye length <2.5 nm (Supporting Information S1). c) Transient-trapping-event-duration histogram normalized by the total number of localizations in the dataset. Only trajectories displaying mobility in their initial and final localizations were considered to ensure that solely complete trapping events were included in the analysis (Supporting Information S4). (d) TE-MSD of all trajectories that span 25–34 frames (Supporting Information S6).

these observations, the pH-dependent experiments were repeated using an unconfined liquid-silica interface. Here, a similar trapping trend was observed with the only difference that no trapping events were detected on the unconfined interface at 20 mM NaOH (Supporting Information S5), highlighting the necessity to characterize trapping in confinement.

We then studied the diffusion of the QDs in 2D pore confinement via mean squared displacement (MSD) analysis and identified their diffusion type. The time-ensemble averaged (TE−)MSD of the sample with transient trapping is nonlinear and its shape suggests that the QDs exhibit anomalous diffusion (see discussion in Supporting Information S6 and Figure S14a). To explore this, we computed the TE-MSD curves of trajectories as a function of their total duration or span. This shows that the flattening of the TE-MSD is a consequence of the positive correlation between the trajectory span and its diffusion constant (Figure S14b–e). Longer displacements of the QD between two subsequent frames are less likely to be linked into a trajectory than shorter ones, which could lead to the observed correlation. This error is exacerbated in conditions with increased short trapping at 7.5 mM NaOH, explaining its anomalous shape. If we exclude this correlation by only considering trajectories with the same span, the TE-MSDs as a function of delay time was found to be linear in both pH conditions, pointing to normal diffusion (Figure 2d). However, the TE-MSD can be linear even though the underlying motion is anomalous. This is known to occur in situations where there is weak ergodicity breaking as a result of time-dependent and space-dependent diffusion.[30,31]

Using a normal diffusion model, we found that the diffusivity and the span of a trajectory were negatively correlated, especially in 7.5 mM NaOH conditions. This is likely an artefact of the linking algorithm, where trajectories with short displacements have a higher probability to be successfully linked (Supporting Information S6). We computed the average diffusivity per time span and weighted it by the number of displacements contributing to that span, obtaining average diffusivities of $1.816\pm0.009\times10^{-12}$ m^{2}s^{-1} and $1.963\pm0.004\times10^{-12}$ m^{2}s^{-1} in 7.5 mM and 20 mM NaOH, respectively. This difference ratio of 7.5 ± 0.6 % can be explained mainly by differences in hydrodynamic size; by tracking QDs in free solution, we found that their size varied with the base concentration (Supporting Information S4). Based on these measured probe sizes, we estimated the diffusivity taking into account the drag force and obtained a theoretical difference of 5.4 % (8.5 %) for a QD positioned at 25 nm (12.5 nm) from the wall (Supporting Information S6).[19] While this seems to be in good agreement with the experiment, we note that three-dimensional particle coordinates would be needed to better understand this difference.

We found that trapping was suppressed in 20 mM NaOH, which prevents blind spots in the pore-space map as a result of removed linking artefacts. Therefore, these conditions were used in another nanofluidic device containing a set of 1D slit-shaped pores (Figure 3a). The different

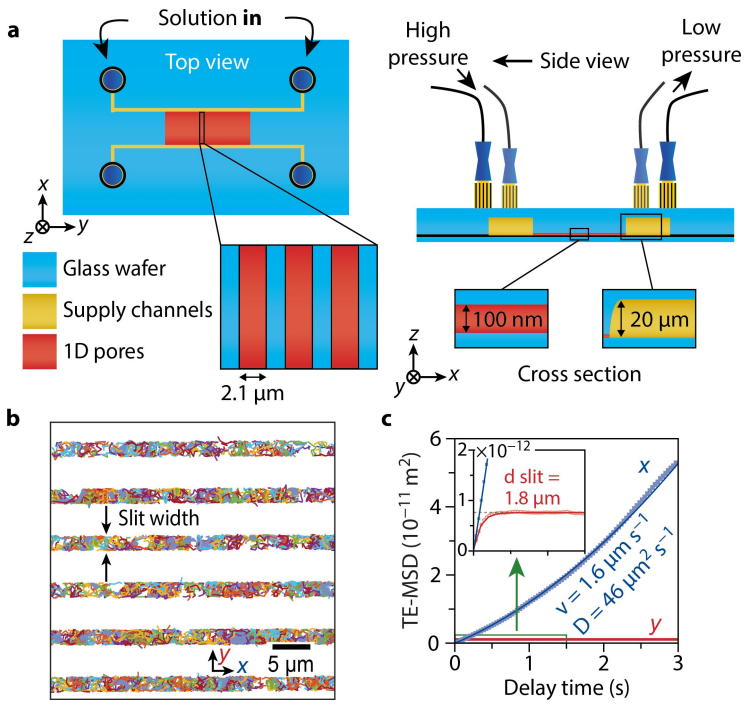

Figure 3. a) Schematic representation of the nanofluidic device containing lithography-patterned 1D pores. b) Overlay of trajectories obtained over 140 s. c) TE-MSD inxand y as a function of time. Solid lines: fit of a directed, *x*, and a confined diffusion model, *y*.[32,33]

pore geometry caused additional confinement within the tracking plane, leaving only one dimension completely open for free diffusion. Unlike in the device containing 2D pores, the chip's in- and outlets were only connected through the 1D pores. By filling the connecting tubing at both ends of the 1D pores at different levels, a flow along the model pores was introduced as result of a pressure difference at the pore ends.

After mapping the pore system (Figure 3b), we used the TE-MSD in the *x*and y directions to characterize probe confinement (Figure 3c). From the *y*-TE-MSD curve, we estimated a pore width of 1.8 µm by fitting the curve with a confinement model.[32,33] The *x*-TE-MSD curve was parabolic and could be described by a directed diffusion model accounting for the flow along the pores' direction.[32,33] This was confirmed by the total displacement of each track, showing preferential movement in *x* (Supporting Information S7).

Finally, we attempted to map the porosity of a single real-life, silica-based polymerization catalyst-support particle via SPT to showcase our method (Figure 4a). A characterization of the particles can be found in the S1.2. The particles are characterized by an extensive macropore network, but they also contain meso- and micropores (mean pore diameter: 23.5 nm; pore volume: 1.6 mL/g; BET surface area: 295 m^2/g All trajectories are in the particle's center, suggesting that most of the accessible porosity is in this region. For comparison we imaged the cross section of

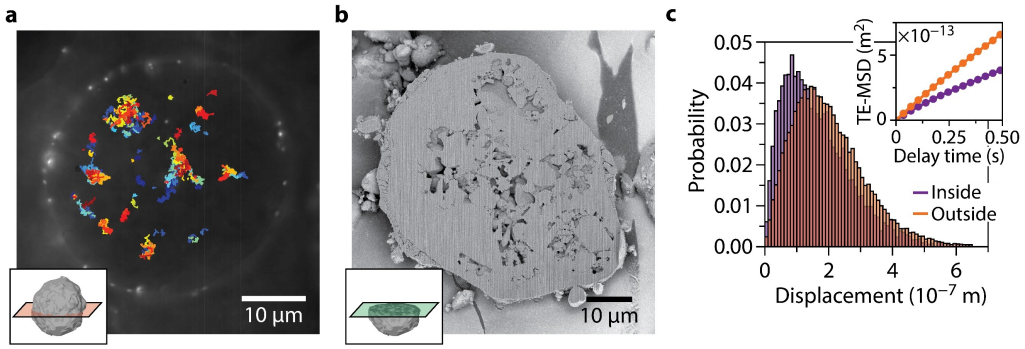

Figure 4. a) Trajectories overlaid with the mean fluorescence intensity obtained within a single olefin polymerization-catalyst particle over 70 s. b) FIB-SEM image of a catalyst particle of the same batch. c) Histogram of displacements of trajectories inside and outside the catalyst particle (35 ms delay time). The TE-MSD is shown in the inset.

another particle of the same batch via focused ion beam milling scanning electron microscopy (FIB-SEM) (Figure 4b). The pore morphology matches qualitatively; there are large pores in the center of the particle which exhibits a denser crust. The QD motion within the particle changed considerably as a result of confinement. Even at a delay time of one frame, the displacements were shorter inside the catalyst than outside (Figure 4c). The limited distance over which a QD can travel before it hits a pore wall as well as the increased hydrodynamic drag in the pore contribute to these shorter displacements. At longer delay times, the mean travelled distance is further reduced by confinement and the TE-MSD curves diverge (inset Figure 4c).

After showing feasibility of the approach, a remaining question is how much tracking time is required to ensure complete pore-space mapping. This cannot be known a priori, as the time needed depends on: 1) the accessibility and size of the pores; 2) their local diffusivities and concentrations; and 3) the desired spatial resolution. To tackle this problem, we propose the following protocol. During a SPT-mapping experiment the pore-space map should be made in parallel. The total mapped porosity (i.e., the covered area or volume) will first grow as a function of time; however, as larger fractions of the pore space are explored, the value will start to plateau, indicating complete pore-space mapping. Once the change in the mapped porosity is smaller than a chosen threshold (linked to the desired mapping resolution), the measurement can be stopped (Supporting Information S9).

Well-defined 2D and 1D model pores have been developed to characterize both diffusion and trapping behavior of confined individual fluorescent probes. The model pore design was pivotal for obtaining long trajectories, allowing a detailed probe characterization. We found that QD trapping could be reduced via tuning the solution pH. Using the 2D model pore, we quantified transient trapping events and found that these were almost completely suppressed in 20 mM NaOH, where the measured diffusivity depended mainly on QD size and not on trapping. Next, we successfully demonstrated the use of non-trapping conditions for pore-space mapping of 1D silica pores and a real-life polymerization catalyst support particle, potentially with resolutions in the order of tens of nanometers. Finally, a protocol to ensure complete porosity exploration in SPT-mapping experiments was introduced.

Further research should be focused on the systematic characterization of the relation between the probe motion behavior (diffusion and trapping) in the model pore and the pore size, shape, and roughness as well as the probe-wall interactions. Moreover, the effects of locally introduced pore defects on mass transport can be studied. This will provide further insights in the factors that promote mass transport through porous solids and/or can be used to validate diffusion models for these materials. The application of our model-pore platform is not limited to pure silica systems since the device can be modified, e.g., for the characterization of fluorescent probes in metal oxide and carbon-based pore environments.

In addition to pore-space mapping, the model pore system shows great potential to study heterogeneous catalyst systems involving small organic molecules operating under diffusion-limited conditions.[34,35] Here, the adsorption behavior of molecules and nanoparticles cannot be compared directly. Although the same forces–including electrostatic interactions, van der Waals forces, and hydrogen bonds–may act on molecules and nanoparticles, their adsorption behavior is qualitatively and quantitatively different. The (pair) interaction energy scales with the size of the molecule or nanoparticle, and with that, its absolute range and strength.[36] Because of the strong forces, nanoparticles often have a more complex interaction potential including a secondary potential energy minimum.[36] Here, a repulsion barrier must be overcome to reach the overall energy minimum, usually causing irreversible adsorption on the catalyst surface. Nevertheless, nanoparticles with a qualitatively similar host affinity as the molecule of interest (i.e., with similar surface functional groups) could be used to study diffusion and adsorption trends. Ultimately, smaller model-pore systems should be employed to investigate molecular motion dynamics in the micro- and mesopore regime.[24,37]

Supporting Information

The authors have cited additional references within the Supporting Information.[38–49]

Acknowledgements

We would like to thank Relinde J. A. van Dijk-Moes (Utrecht University, UU) for transmission electron microscopy on the QDs and Arnout Imhof (UU) for fruitful discussions. This work was supported by the Netherlands Center for Multiscale Catalytic Energy Conversion (MCEC), an NWO Gravitation Program funded by the Ministry of Education, Culture and Science of the Government of the Netherlands. F.M. also acknowledges funding from the Netherlands Organization for Scientific Research (NWO) VIDI Grant (No. 723.015.007).

Conflict of Interest

The authors declare no conflict of interest.

Data Availability Statement

The data will be made available in a repository hosted by Utrecht University.

Keywords: Diffusion · Nanofluidics · Porosity Characterization · Single Particle Tracking · Single-Molecule Localization Microscopy

[1] Y. Liu, F. Meirer, C. M. Krest, S. Webb, B. M. Weckhuysen, *Nat. Commun.* **2016**, *7*, 12634.
[2] D. H. Everett, *Pure Appl. Chem.* **1972**, *31*, 577–638.
[3] E. T. C. Vogt, B. M. Weckhuysen, *Chem. Soc. Rev.* **2015**, *44*, 7342–7370.
[4] G. T. Whiting, N. Nikolopoulos, I. Nikolopoulos, A. D. Chowdhury, B. M. Weckhuysen, *Nat. Chem.* **2019**, *11*, 23–31.
[5] G. T. Whiting, S. H. Chung, D. Stosic, A. D. Chowdhury, L. I. Van Der Wal, D. Fu, J. Zecevic, A. Travert, K. Houben, M. Baldus, B. M. Weckhuysen, *ACS Catal.* **2019**, *9*, 4792–4803.
[6] S. Mitchell, N. L. Michels, K. Kunze, J. Pérez-Ramírez, *Nat. Chem.* **2012**, *4*, 825–831.
[7] J. C. da Silva, K. Mader, M. Holler, D. Haberthür, A. Diaz, M. Guizar-Sicairos, W. C. Cheng, Y. Shu, J. Raabe, A. Menzel, J. A. Vanbokhoven, *ChemCatChem* **2015**, *7*, 413–416.
[8] D. A. M. De Winter, F. Meirer, B. M. Weckhuysen, *ACS Catal.* **2016**, *6*, 3158–3167.
[9] R. Mayorga-González, M. Rivera-Torrente, N. Nikolopoulos, K. W. Bossers, R. Valadian, J. Yus, B. Seoane, B. M. Weckhuysen, F. Meirer, *Chem. Sci.* **2021**, *12*, 8458–8467.
[10] F. Meirer, B. M. Weckhuysen, *Nat. Rev. Mater.* **2018**, *3*, 324–340.
[11] N. Naredi-Rainer, J. Prescher, A. Hartschuh, D. C. Lamb, *Fluorescence Microscopy*, Wiley-VCH, Weinheim, **2017**, pp. 165–202.
[12] D. Fu, J. J. E. Maris, K. Stanciakova, N. Nikolopoulos, O. Heijden, L. D. B. Mandemaker, M. E. Siemons, D. Salas Pastene, L. C. Kapitein, F. T. Rabouw, F. Meirer, B. M. Weckhuysen, *Angew. Chem. Int. Ed.* **2022**, *61*, e202114388.
[13] B. Dong, N. Mansour, T.-X. Huang, W. Huang, N. Fang, *Chem. Soc. Rev.* **2021**, *50*, 6483–6506.
[14] J. J. E. Maris, D. Fu, F. Meirer, B. M. Weckhuysen, *Adsorption* **2021**, *27*, 423–452.
[15] C. Hellriegel, J. Kirstein, C. Bräuchle, *New J. Phys.* **2005**, *7*, 23–23.
[16] A. Zürner, J. Kirstein, M. Döblinger, C. Bräuchle, T. Bein, *Nature* **2007**, *450*, 705–708.
[17] F. C. Hendriks, F. Meirer, A. V. Kubarev, Z. Ristanović, M. B. J. Roeffaers, E. T. C. Vogt, P. C. A. Bruijnincx, B. M. Weckhuysen, *J. Am. Chem. Soc.* **2017**, *139*, 13632–13635.
[18] P. Chen, X. Zhou, N. M. Andoy, K. S. Han, E. Choudhary, N. Zou, G. Chen, H. Shen, *Chem. Soc. Rev.* **2014**, *43*, 1107–1117.
[19] H. J. Keh, P. Y. Chen, *Chem. Eng. Sci.* **2001**, *56*, 6863–6871.
[20] P. Frantz, S. Granick, *Phys. Rev. Lett.* **1991**, *66*, 899–902.
[21] J. F. Douglas, H. E. Johnson, S. Granick, *Science* **1993**, *262*, 2010–2012.
[22] J. Michaelis, C. Bräuchle, *Chem. Soc. Rev.* **2010**, *39*, 4731–4740.
[23] T. Lebold, J. Michaelis, C. Bräuchle, *Phys. Chem. Chem. Phys.* **2011**, *13*, 5017–5033.
[24] G. B. Salieb-Beugelaar, J. Teapal, J. Van Nieuwkasteele, D. Wijnperlé, J. O. Tegenfeldt, F. Lisdat, A. van den Berg, J. C. T. Eijkel, *Nano Lett.* **2008**, *8*, 1785–1790.
[25] S. L. Eichmann, S. G. Anekal, M. A. Bevan, *Langmuir* **2008**, *24*, 714–721.
[26] B. Lin, J. Yu, S. A. Rice, *Phys. Rev. E* **2000**, *62*, 3909–3919.
[27] M. J. Saxton, *Biophys. J.* **1993**, *64*, 1766–1780.
[28] R. Simson, E. D. Sheets, K. Jacobson, *Biophys. J.* **1995**, *69*, 989–993.
[29] M. Vrljic, S. Y. Nishimura, W. E. Moerner, *Methods Mol. Biol.* **2007**, *398*, 193–219.
[30] C. Manzo, M. F. Garcia-Parajo, *Rep. Prog. Phys.* **2015**, *78*, 124601.
[31] R. Metzler, J. H. Jeon, A. G. Cherstvy, E. Barkai, *Phys. Chem. Chem. Phys.* **2014**, *16*, 24128–24164.
[32] J. J. E. Maris, F. T. Rabouw, B. M. Weckhuysen, F. Meirer, *Sci. Rep.* **2022**, *12*, 9595.
[33] H. Qian, M. P. Sheetz, E. L. Elson, *Biophys. J.* **1991**, *60*, 910–921.
[34] G. De Cremer, M. B. J. Roeffaers, E. Bartholomeeusen, K. Lin, P. Dedecker, P. P. Pescarmona, P. A. Jacobs, D. E. De Vos, J. Hofkens, B. F. Sels, *Angew. Chem. Int. Ed.* **2010**, *49*, 908–911.
[35] G. Fleury, M. B. J. Roeffaers, *ACS Catal.* **2020**, *10*, 14801–14809.
[36] J. N. Israelachvili, *Intermolecular and Surface Forces*, Academic Press, Cambridge, **2011**.
[37] A. Esfandiar, B. Radha, F. C. Wang, Q. Yang, S. Hu, S. Garaj, R. R. Nair, A. K. Geim, K. Gopinadhan, *Science* **2017**, *358*, 511–513.
[38] M. J. Werny, J. Zarupski, I. C. ten Have, A. Piovano, C. Hendriksen, N. H. Friederichs, F. Meirer, E. Groppo, B. M. Weckhuysen, *JACS Au* **2021**, *1*, 1996–2008.
[39] M. J. Bergman, J. S. Pedersen, P. Schurtenberger, N. Boon, *Soft Matter* **2020**, *16*, 2786–2794.
[40] N. Sahai, D. A. Sverjensky, *Geochim. Cosmochim. Acta* **1997**, *61*, 2801–2826.
[41] K. B. Krauskopf, *Geochim. Cosmochim. Acta* **1956**, *10*, 1–26.
[42] H. Wu, D. K. Schwartz, *Acc. Chem. Res.* **2020**, *53*, 2130–2139.
[43] L. C. Katrukha, E. A. Cloin, B. Teeuw, J. Kapitein, **2017**. Detection of Molecules plugin for ImageJ. Utrecht University https://github.com/ekatrukha/DoM_Utrecht.
[44] P. Dedecker, S. Duwé, R. K. Neely, J. Zhang, *J. Biomed. Opt.* **2012**, *17*, 126008.
[45] J. C. Crocker, D. G. Grier, *J. Colloid Interface Sci.* **1996**, *179*, 298–310.
[46] E. A. Katrukha, M. Mikhaylova, H. X. van Brakel, P. M. van Bergen en Henegouwen, A. Akhmanova, C. C. Hoogenraad, L. C. Kapitein, *Nat. Commun.* **2017**, *8*, 14772.
[47] M. J. Saxton, **2007**, 400 pp. 295–321, https://doi.org/10.1007/978-1-59745-519-0_20.
[48] A. Volk, C. J. Kähler, *Exp. Fluids* **2018**, *59*, 75.
[49] J. Janzen, X. Song, D. E. Brooks, *Biophys. J.* **1996**, *70*, 313–320.

Manuscript received: September 27, 2023
Accepted manuscript online: December 1, 2023
Version of record online: December 1, 2023